Reactive and Functional Polymers 208 (2025) 106156

Contents lists available at ScienceDirect

Reactive and Functional Polymers

journal homepage: www.elsevier.com/locate/react

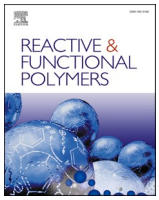

Synthesis of size-controlled poly(vinyldiaminotriazine) nanoparticles for enhanced hydrogen bonding adsorption of horseradish peroxidase

Xiaotao Wang [a,*], Chuan Xu [a], Feiyang Xiao [a], Xiangning Yan [a], Chak-Yin Tang [b], Huiling Guo [a,*], Wing-Cheung Law [b,*]

[a] Hubei Provincial Key Laboratory of Green Materials for Light Industry, Collaborative Innovation Center for Green Light-weight Materials and Processing, School of Materials Science and Engineering, Hubei University of Technology, Wuhan 430068, PR China
[b] Department of Industrial and Systems Engineering, The Hong Kong Polytechnic University, Hung Hom, Kowloon, Hong Kong, China

ARTICLE INFO

Keywords:
Poly(2-vinyl-4,6-diamino-1,3,5-triazine)
Semi-continuous precipitation polymerization
polymer nanoparticles
Adsorption
Horseradish peroxidase

ABSTRACT

Physically adsorbing proteins through functional polymeric nanoparticles hold great potential for a variety of applications. Achieving strong and stable adsorption via hydrogen bonding in aqueous phases is challenging due to the interference from water molecules. The monomer 2-vinyl-4,6-diamino-1,3,5-triazine (VDAT) not only provides donor and receptor sites for hydrogen bonding but also possesses an apolar nature that can help prevent water molecules from interfering with these bonding sites. In this work, poly(vinyldiaminotriazine) nanoparticles (PVDAT) with sizes ranging from approximately 50 nm to 240 nm were synthesized through semi-continuous precipitation polymerization in water. The formation mechanism of PVDAT, including particle nucleation and growth stages, was investigated. VDAT oligomers aggregated to form a core and subsequently grew by adsorbing additional VDAT oligomers. Adsorption studies of PVDAT on horseradish peroxidase (HRP) demonstrated stable physical adsorption facilitated by hydrogen bonding between PVDAT and the enzyme in the aqueous phase. The adsorption of HRP by PVDAT followed the Langmuir model of single-layer adsorption, with a maximum adsorption capacity of 13.80 mg/g and a retention of enzymatic activity of ~74.99 %. This innovative approach aims to enhance the precision and efficacy of protein separation and extraction, as well as the efficiency of enzyme immobilization.

1. Introduction

Proteins are bioactive macromolecules that play crucial roles in biological processes and are fundamental to life. Understanding the adsorption behavior and mechanisms of proteins with various materials is essential for applications such as protein separation, extraction, and enzyme immobilization [1,2]. However, the adsorption process can often compromise the conformational stability of proteins, leading to alterations in their structure and function. For instance, Zhang et al. [3] developed a polydopamine (PDA)-coated biocatalytic membrane for protein loading via covalent bonding, which adversely affected the stability of protein conformation post-loading. Similarly, Matsuura et al. [4] studied the electrostatic adsorption of water-soluble proteins onto carbon nanotubes, but the stringent charge requirements posed challenges in preserving protein conformation. Moreover, electrostatic interactions are sensitive to variations in pH and ionic strength, further complicating the adsorption process.

H-bonding is a strong physical interaction with high directionality and hence, has attracted increasing interests for both academia research and industrial development as an effective driving force for physical adsorptions [5–7]. The study of H-bonding force and its adsorption properties have attracted great interests. Protein adsorptions are ideally conducted in aqueous media because they are usually inactivated in organic solvents. However, achieving strong and stable hydrogen bonding in aqueous environments is challenging due to the competitive nature of water molecules, which can weaken or disrupt the hydrogen bonds between proteins and functional polymers [8].

Molecular biology suggests that H-bonding as a non-covalently bonded is primarily influenced by the atoms or groups within the amino acid units and their ligands [9]. The flexibility of these groups allows for optimal binding site accessibility through chain folding. Additionally, adjacent segments of the polypeptide chain can restrict water molecules from entering the binding site, enhancing the strength of hydrogen bonding between the protein and the ligand [10]. Thus, the

* Corresponding authors.
E-mail addresses: xiaotaowang@hbut.edu.cn (X. Wang), guoguo0302@126.com (H. Guo), roy.law@poly.edu.hk (W.-C. Law).

https://doi.org/10.1016/j.reactfunctpolym.2025.106156
Received 27 April 2024; Received in revised form 6 January 2025; Accepted 7 January 2025
Available online 12 January 2025
1381-5148/© 2025 The Authors. Published by Elsevier B.V. This is an open access article under the CC BY license (http://creativecommons.org/licenses/by/4.0/).

restriction of water plays a critical role in the specific adsorption of biological macromolecules, synergistically enhancing hydrogen bonding interactions. This synergistic effect of hydrophobic hydrogen bonds facilitates improved binding between proteins and functional monomers.

The VDAT monomer has both donor and receptor for H-bonding sites (Fig. 1) and exhibits very low water solubility at room temperature. This is probably attributed to its unique physiochemical characteristics which enable multiple intermolecular hydrogen bands that are too strong to be broken in neither water, nor the organic solvents. The special structure of VDAT favors an effective protein adsorption through H-bonding sites in aqueous systems, which is expected to minimize the effects of water molecules [11–13] (Fig. 2). VDAT contains multiple amino groups (−NH2), which can serve as the H-bond donors while the triazine rings act as the H-bond acceptors. This configuration facilitates the formation of a stable network of hydrogen bonds between PVDAT nanoparticles and proteins, such as horseradish peroxidase (HRP). In addition to hydrogen bonding, the hydrophobic regions of PVDAT facilitate the interaction with HRP. The presence of hydrophobic effects in aqueous solutions promotes the formation of the protein complex and avoids the interference from water molecules. For effective physical adsorptions, micro- or nanoparticles with large specific surface areas and flexibility are preferred to meet various application needs [14,15]. However, the traditional synthetic methods are not suitable for synthesizing PVDAT particles, limited by the poor solubility of solid VDAT in both water and organic solvents.

In this work, we synthesized monodispersed PVDAT nanoparticles through semi-continuous precipitation polymerization in the aqueous phase, allowing for precise control over particle size. We investigated the formation mechanism of PVDAT particles and explored the adsorption behavior and mechanisms of HRP in aqueous media. Notably, the hydrogen bonding between PVDAT and proteins remains unaffected by water, resulting in an impressive enzymatic activity retention of ~74.99 %. This study might be widely used in sewage treatment [16,17], medical diagnostic assay [18] and enzyme biosensor [19].

2. Experimental

2.1. Materials

2,2′-azobis (2-methylpropionamidine) dihydrochloride (V50) was purchased from Shanghai Aladdin Chemistry Co. Ltd. VDAT was synthesized in our laboratory according to the method in reference [20]. Phosphate buffered saline (PBS) was prepared from sodium dihydrogen phosphate and disodium hydrogen phosphate which were both purchased from Sinopharm Chemical Reagent Co. Ltd. Dimethyl sulfoxide (DMSO, AR)and hydrogen peroxide aqueous solution (H_2O_2, 30 %) were also purchased from Sinopharm Chemical Reagent Co. Ltd. Horseradish peroxidase (HRP, RZ:>3.0) and 3,3′,5,5’-Tetramethylbenzidine (TMB, 99.0 %) were obtained from Shanghai Macklin Biochemical Technology Co. Ltd., and stored in a refrigerator prior to use. Distilled deionized (DDI) water was used in all experiments, and all HRP solutions were prepared by dissolving in PBS.

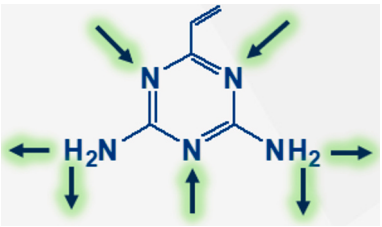

Fig. 1. VDAT structure and potential sites for H-bonding.

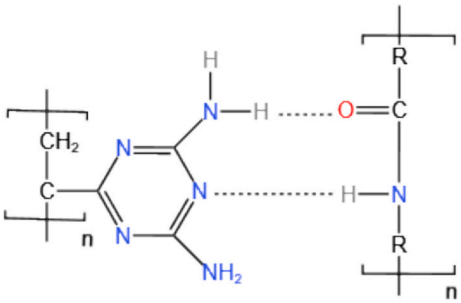

Fig. 2. Schematic diagram of the hydrogen bonding binding site of PVDAT particles to the peptide bone in protein (The PVDAT model is on the left and peptide bone model is on the right).

2.2. Synthesis of PVDAT nanoparticles with controllable particle size

PVDAT nanoparticles were prepared by semi-continuous aqueous precipitation polymerization method in a 100 mL four-necked reactor which was immersed in 80 °C oil-bath and equipped with a mechanical stirrer at 200 rpm, a water-cooled condenser, nitrogen inlet and outlet. VDAT (0.4 g) and V50 (0.004 g) were dissolved in 7.5 mL DMSO and 7.5 mL DDI water, respectively in two reservoirs which were separately connected to the two liquid feed inlets of the reactor by using two rubber tubes of a multi-channel peristaltic pump. In the reactor, deoxygenated 25 mL DDI water by slow nitrogen bubbling for 30 min. Then, take 0.75 mL V50 solution from the V50 reservoir and added to the reactor as one shot. To make up the total volume of 0.75 mL in theV50 reservoir, 0.75 mL DDI water was added. After that, the peristaltic pump was started to continuously feed the VDAT solution andV50 solution to the reactor at a flow rate of 21.82 μL/min.

To collect PVDAT nanoparticles with different particle sizes, approximately 2.0 mL samples were taken from the reactor at different reaction timepoints until the VDAT and V50 solutions were fed completely. The collected samples were purified by dialysis against DDI water with water change every four hours for three times. Finally, the purified PVDAT nanoparticles were stored at room temperature for further use.

2.3. Adsorption of HRP by PVDAT nanoparticles

2.3.1. pH and ionic strength studies

PBS buffers with a pH range of 6.0 to 8.0 and an ionic strength range of 0.1–1.0 mol/L were prepared for use. PVDAT nanoparticles of about 150 nm diameter were used for the pH and ionic strength studies. HRP solutions in PBS with a concentration range of 50–2000 μg/mL were mixed with the purified nanoparticle dispersion with a solid content of 10 mg/mL by using a mechanical shaker (TS-1). Then, the mixtures were centrifuged by using a desktop high-speed centrifuge (TLL-C) at 10000 rpm for 10 min, and the supernatants were collected and filtered off using 0.45-ìm PES Syringe Filters. Absorbance at 403 nm wavelength of HRP in the supernatants were measured with an UV–visible spectrophotometer (Hitachi U3900), and the residual HRP concentrations in the supernatants were calculated by using the corresponding calibration equations for HRP. Finally, HRP adsorptions were worked out from the residual HRP concentrations.

2.3.2. Adsorption capacity and kinetics

The same PVDAT nanoparticle dispersion described in the immediate above section were mixed with HRP solutions in PBS with a concentration range of 100–1500 μg/mL, where the PBS had a pH of 6.0 and an ionic strength of 0.1 mol/L. The methods of mixing, separation and HRP adsorption measurements were the same as described in the immediate above section. Four isotherm models of Langmuir, Freundlich and Temkin, expressed in Eqs. (1) to (3), were employed to fit the

equilibrium data and obtain the key adsorption constants [21–23].

$$\frac{C_e}{q_e} = \frac{1}{q_m \bullet K_L} + \frac{C_e}{q_m} \quad (1)$$

$$lnq_e = lnK_F + \frac{1}{n} \cdot lnCe \quad (2)$$

$$q_e = B \cdot lnA + B \cdot lnCe \quad (3)$$

where C_e (μg/mL) is the equilibrium concentration, q_e (mg/g) is the adsorption capacity at equilibrium, q_m (mg/g) is the maximum monolayer adsorption capacity calculated by the Langmuir model, K_L is the Langmuir adsorption constant. The characteristics of the Langmuir isotherm can also be expressed in a term of equilibrium parameter (R_L), $R_L = 1/(1 + K_L \cdot C_0)$, where C_0 is the initial concentration. K_F and n are Freundlich constants, $K_F$represents the relative adsorption capacity of adsorbent, and n is related with adsorption intensity. $B$is the Temkin isotherm constant and A is the Temkin isotherm energy constant.

The Langmuir isotherm assumes that the adsorption cannot proceed beyond monolayer coverage of adsorbate over a homogeneous adsorbent surface [24,25]. The Freundlich model is an empirical expression used to describe both the heterogeneous surfaces and multilayer adsorption. The Temkin isotherm assumes that the binding energy is distributed uniformly for the adsorption.

Under the same conditions, adsorption kinetic studies were carried out under the HRP concentration of 100 μg/mL, and the adsorption time varied between 5 and 90 min.

2.3.3. Adsorption of HRP by PVDAT nanoparticles with different particle sizes

PVDAT nanoparticles with a particle size of 120 nm, 150 nm and 240 nm were mixed with HRP solutions in PBS (pH = 6, ionic strength 0.1 M) with a concentration range of 100–800 μg/mL, and then carried out according to the above method.

2.3.4. Adsorbed HRP activity studies

ELISA method was used to analyze activity of the adsorbed HRP through the HRP, TMB, and H_2O_2 reactions. PBS buffer with pH of 6 and ionic strength of 0.1 M was prepared. The H_2O_2 solution (30 %) was diluted 1000 times, and 2.5 g/L TMB solution was prepared with ethanol.

0.01 mL of 1 μg/mL HRP solution, 0.2 mL of TMB solution and 0.78 mL of PBS dispersion were mixed in a centrifuge tube, then 0.01 mL of H_2O_2 solution was added and the chronograph was started. The mixed solution was shaken quickly and transferred to a cuvette, and the absorbance changes with wavelength at different times were recorded using the UV–visible spectrophotometer.

Enzyme activity standard curve was drawn. 1–10 μg/mL HRP solution was mixed with TMB and H_2O_2according to the above method and transferred to the cuvette respectively. The curve of absorbance at a wavelength of 650 nm over time was tested by UV–visible spectrophotometer.

The HRP solutions with an original concentration range of 100–1500 μg/mL were adsorbed by PVDAT nanoparticles, and the PVDAT nanoparticles adsorbed with different concentrations of HRP were redispersed into the PBS. Immediately afterwards, 0.01 mL the above dispersion with different concentrations was mixed with TMB and H_2O_2, transferred to the cuvette and tested by the UV–visible spectrophotometer according to the above method. Finally, the content of active HRP was calculated according to the comparison between the enzyme reaction process curve and enzyme activity standard curve.

3. Results and discussion

3.1. Synthesis of PVDAT nanoparticles and particle size control

PVDAT nanoparticles were prepared by semi-continuous aqueous precipitation polymerization. V50 was used as a cationic initiator to provide long range electrostatic repulsion between the nanoparticles and ensure stability of the PVDAT nanoparticles during the polymerization and storage.

Due to VDAT physiochemical character, DMSO was used to dissolve VDAT for the nanoparticle synthesis. To remove the residual DMSO in the collected PVDAT nanoparticle samples, four different purification methods were investigated and the DLS results of a PVDAT nanoparticle sample after the purification were compared in Fig. 3**.** Only the dialysis method had little impact on the average diameter and polydispersity of the PVDAT nanoparticles, whereas the freeze-dry, centrifugation and vacuum-dry methods resulted in agglomerates of approximately 300 nm, 362 nm, and 405 nm respectively, in addition to a population of the original nanoparticles. This was not surprising given that the positively charged nanoparticles were kept separate throughout the dialysis purification, whilst the nanoparticles were forced to be compacted during the other three methods of purification and became difficult to be fully redispersed. Therefore, all the PVDAT nanoparticles used for the studies reported in this article were purified by the dialysis method.

Fig. 4 shows Zeta potential results of the PVDAT nanoparticles before and after the dialysis purification. After removing DMSO, the zeta potential increased from +38.89 mV to +51.97 mV. The purified PVDAT nanoparticles had good stability in pure water and no visible change upon leaving to stand at room temperature for over 12 months.

SEM image of the above discussed PVDAT nanoparticle sample is shown in Fig. 5(a). The nanoparticles were uniform with an average particle size of about 150 nm. DLS results of the same sample is shown in Fig. 5(b), indicating an average particle size of 155 nm and a polydispersity of 0.005.

As reported in our previous publications [26], the particle formation mechanism is depicted in Fig. 6. Briefly, V50 primary free-radicals initiated chain reactions of VDAT in the aqueous media, and the formed oligomers precipitated out to form nuclei as their solubility rapidly decreased with increasing molecular weight. These nuclei grew by capturing newly formed VDAT oligomers/polymers as VDAT and V50 were continuously fed into the reactor. The continuous capture of newly formed oligomers/polymers also resulted in accumulation of the positive charges at the particle surfaces. Compared with the traditional precipitation polymerization proposed by Stöver et al. [27], the number

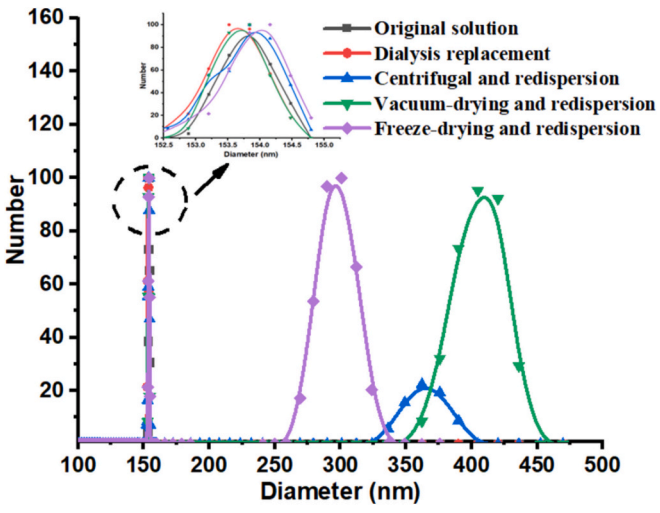

Fig. 3. DLS results of PVDAT nanoparticle sample before and after purification of different methods.

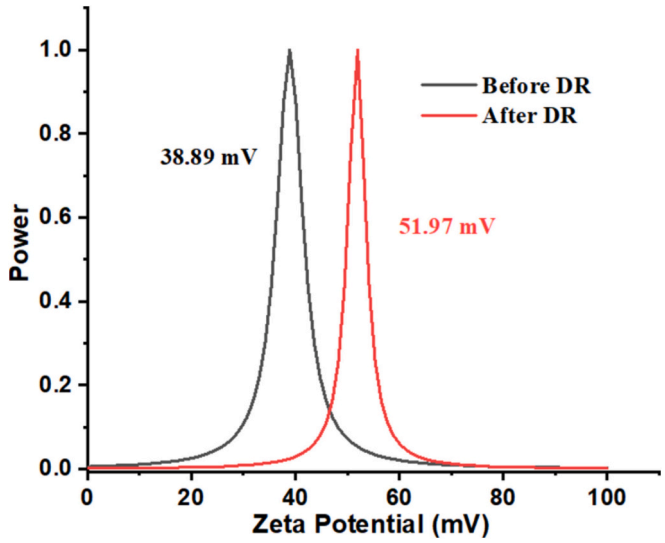

Fig. 4. Zeta potential of PVDAT nanoparticles before and after DR.

ratio of PVDAT nuclei or particles to the newly formed oligomers/polymers was relatively large throughout the course of particle growth because only a small quantities of VDAT was present in the reaction system at any timepoints. Therefore, the newly formed oligomers/polymers were likely to be captured by the large number of growing nuclei or particles rather than forming new nuclei. As a result, the particle size distribution was kept narrow while the particle size gradually increased with the continuous monomer feeding.

The above hypothesis was verified by the particle analysis results of samples collected at different polymerization timepoints. Fig. 7 shows variation of DLS results of PVDAT nanoparticles with varied quantities of the monomer feed. The nanoparticles grew rapidly at the early stages and then slowed down with increasing the monomer quality. This is a common phenomenon as the particle diameter increase is always faster for smaller particles.

SEM images in Fig. 8 reveal the uniform PVDAT nanoparticles with increased particle size at varied quantities of VDAT. It is noteworthy that some small particles were visible in Fig. 8 (e) and Fig. 8 (f). These small particles likely resulted from the newly formed oligomers/polymers at the late stages of polymerization. This could be attributed to the slow-down in capturing the positively charged oligomers/polymers by the unlikely charged existing particles as their surface charge density increased to a certain degree. This observation was confirmed by repeating the experimentations.

The nanoparticles collected at different polymerization timepoints (with varied VDAT feed quantities) had not only uniform particle size, but also good stability.It remains colloidally stable after several days This provided opportunity to synthesis PVDAT nanoparticles with controllable particle size in a range of approximately 50 nm to 240 nm. Fig. 9 shows results of PVDAT nanoparticles with an average diameter of about 50 nm. Three different size PVDAT nanoparticles were prepared and used for study of the particle size effect on HRP adsorption as presented in the following section.

3.2. Adsorption of HRP by PVDAT nanoparticles

The solution acidity and ionic strength are important parameter which are highly affecting the adsorption process [28,29]. Effects of pH (6 to 8) and ionic strength (0.1 to 1.0 mol/L) on the adsorption were studied by using the PVDAT nanoparticles with an average particle size of about 150 nm. The adsorption capacities were worked out from the residual HRP quantities which were calculated from 403 nm absorbance

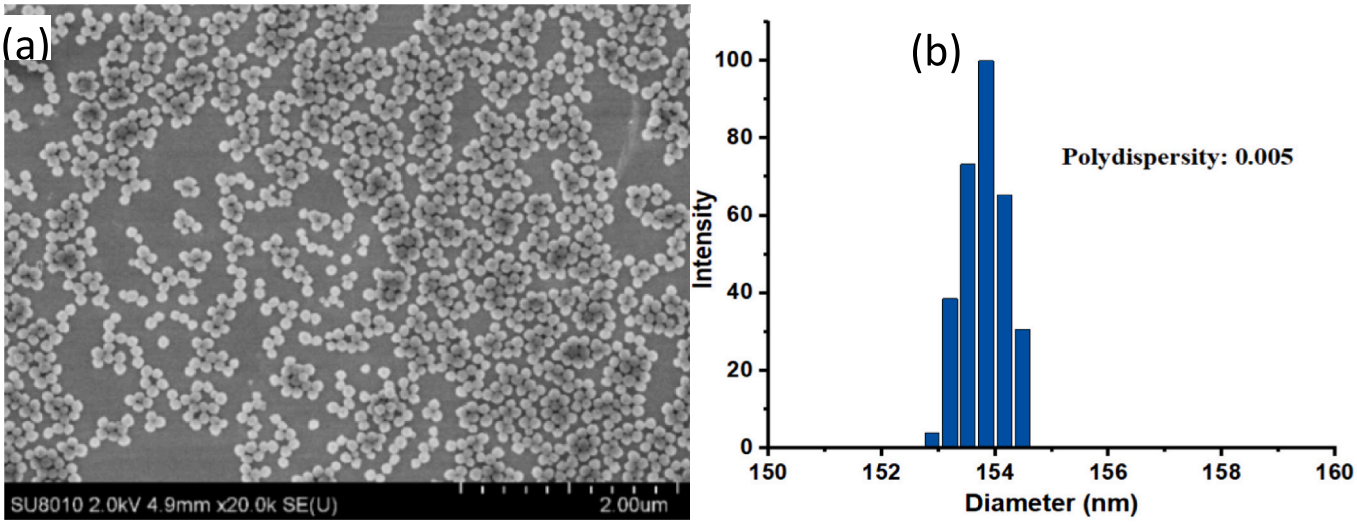

Fig. 5. SEM images and DLS results of one PVDAT nanoparticle sample.

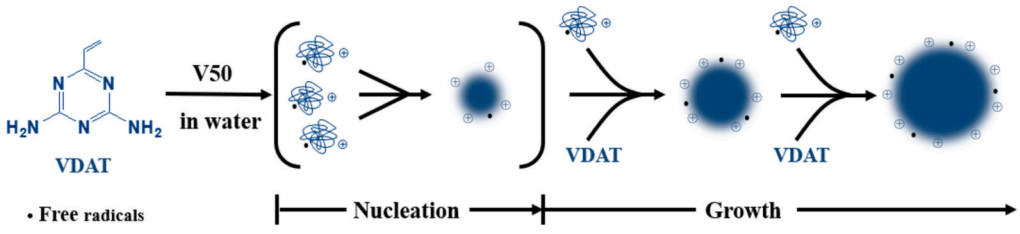

Fig. 6. The formation mechanism of PVDAT nanoparticles.

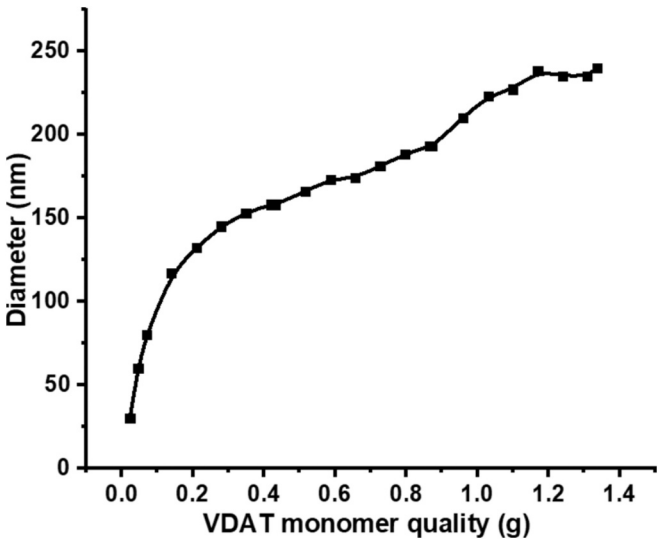

Fig. 7. Particle size growth of PVDAT nanoparticles.

of the HRP supernatants by using the corresponding standard curve under the pH or ionic strength conditions (see Supplementary Information, Fig. S1). The pH range was purposely studied across HRP isoelectric point (7.2). As shown in Fig. 10(a), the HRP adsorption occurred at all the pH conditions. At pH 6, the HRP surfaces were positively charged and hence, there would be electrostatic repulsion between HRP and the PVDAT nanoparticles. The detected HRP adsorption must be attributed to the effective H-bonding which was greater than the electrostatic repulsion. The increased HRP adsorption as the pH changed from 6 to 8was expected given that the charge state of HRP surfaces changed from positive to negative as the pH rose above the HRP isoelectric point, and the electrostatic interaction between HRP and the positively charged PVDAT nanoparticles altered from repulsion to attraction.

The positive charges at the HRP surfaces changed to negative charge, and the amount of negative charge will gradually increase. It is worth noting that the pl of HRP is 7.2. When the pH is lower than 7.2, the surface of HRP is positively charged, and there would be electrostatic repulsion between PVDAT nanoparticles, but HRP was still adsorbed, which proves that PVDAT nanoparticles can form an effective hydrogen bond with HRP, and the hydrogen bond is greater than electrostatic. Fig. 10(b) showed that the adsorption amount of HRP increased with the

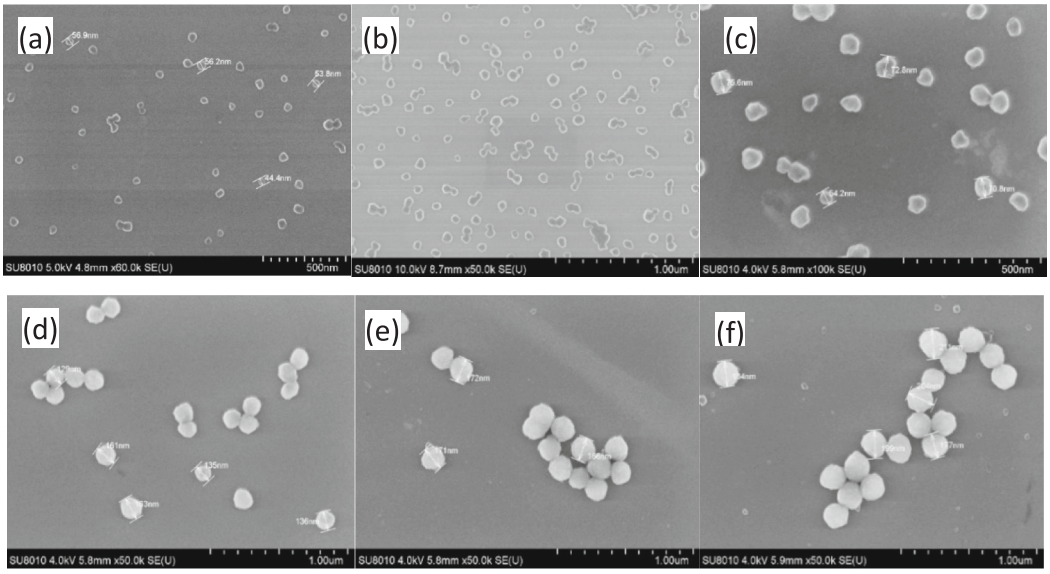

Fig. 8. SEM images of PVDAT nanoparticle with VDAT feed mass: (a) 0.023 g, (b) 0.046 g, (c) 0.070 g, (d) 0.433 g, (e) 0.866 g, (f) 1.200 g.

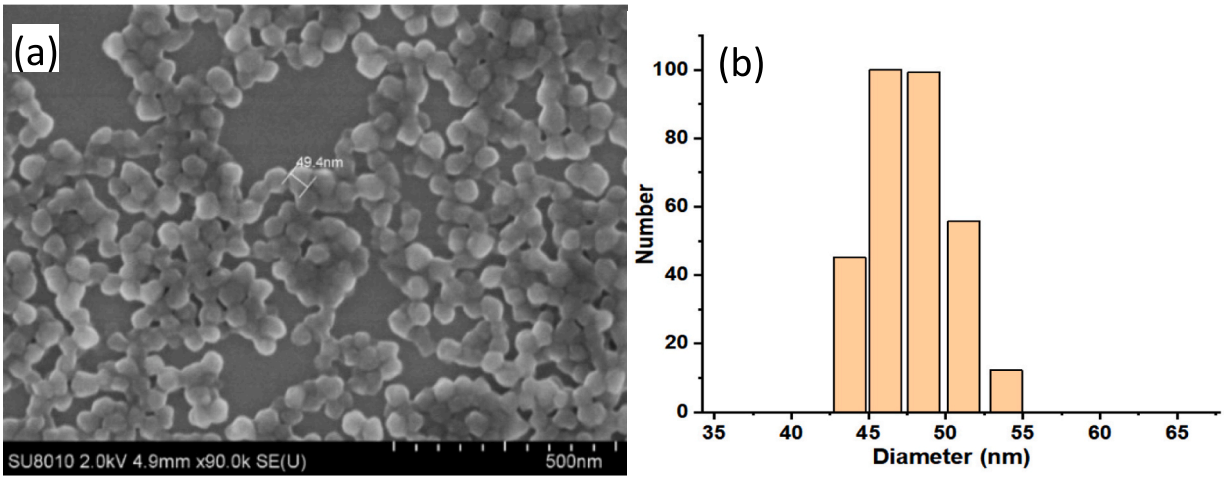

Fig. 9. SEM image and DLS result, respectively of another PVDAT nanoparticle sample which was collected at the early stage (20 min) of VDAT and V50 feeding.

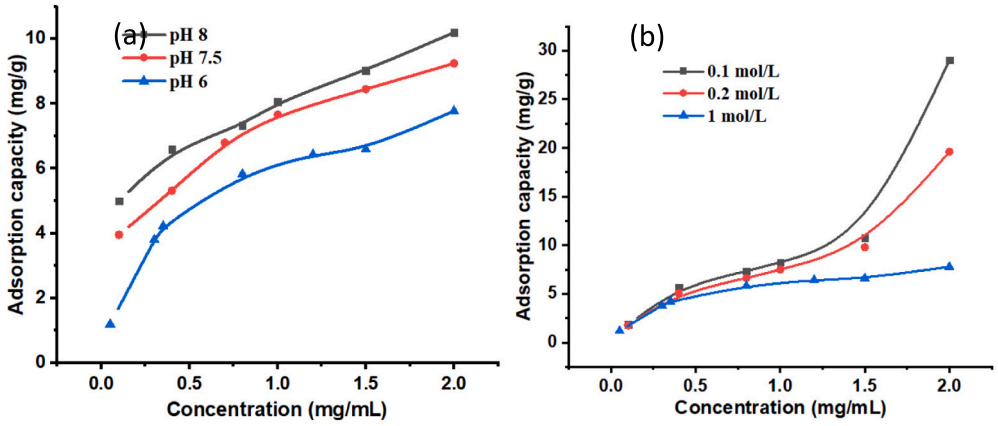

Fig. 10. HRP adsorptions under: (a) Different pH at 1.0moL/L ionic strength, (b) Different ionic strength at pH 6.

decrease of ionic strength. The main reason is that PVDAT nanoparticles are positively charged, when the ionic strength is relatively high, the shielding effect on the surface charge of the particles will be greater. Which will cause the stability of the nanoparticles to decrease, and even agglomeration deposition will occur. Notably, the adsorption capacity of HRP under different ionic strengths within a certain concentration range increased slowly with the increase of the concentration, but when the concentration rose to 2 mg/mL, the adsorption capacity all appeared to rise sharply. It is presumed that this may be because when the concentration of HRP reaches a certain value, the enzyme will be deactivated, and the multilayer will be adsorbed on the particle surface. And this has been confirmed in the discussion of enzyme activity in the next section.

In order to fully evaluate the adsorption capacity of PVDAT nanoparticles to HRP, the adsorption capacity was tested. The initial concentration of the adsorbate has a very important influence on the adsorption process [30]. Under the conditions of pH 6 and ionic strength of 0.1 mol/L, if the concentration is too high, HRP will be inactivated. Thus, the initial concentration of HRP was selected to be 0.1–1.5 mg/mL, and the adsorbed protein was calculated by UV–visible spectrophotometer. As shown in Fig. 11, the adsorption capacity of PVDAT nanoparticles on HRP gradually increased with the increase of HRP concentration. When the protein concentration was lower than 0.4 mg/mL, the adsorption rate was faster, and when the protein concentration was higher than 0.4 mg/mL, the adsorption rate gradually decreased. This may be because the adsorption is about to reach equilibrium.

The adsorption isotherm equation can be used not only to evaluate the adsorption capacity of the adsorbent, but also to determine the interaction between the adsorbent and the adsorbent [31,32]. The three adsorption isotherm equations of Langmuir (C_e/q_e to C_e), Freundlich (lnq_e to lnC_e) and Temkin (q_e to lnC_e) were used to fit the HRP adsorption capacity as shown in Fig. 12. From the correlation coefficient of each adsorption model, the Langmuir model was the best fitting equation describing the adsorption of HRP, with the highest correlation coefficient value ($R^2 = 0.993$). This indicated that HRP may form a single layer of adsorption on the surface of PVDAT nanoparticles, and from the correlation coefficient of the Temkin equation ($R^2 = 0.989$), it can be seen that the surface of PVDAT nanoparticles has the same adsorption capacity. According to the Langmuir fitting equation, the maximum adsorption capacity of PVDAT nanoparticles for HRP can reach 13.80 mg/g, the adsorption of micron-scale PVDAT microspheres prepared by Liu et al. [33] is only 8.68 mg/g, which fully indicates that the adsorption capacity of nanoparticles is stronger than that of micron particles. In addition, the Langmuir equilibrium parameter R_L represents the adsorption properties: irreversible ($R_L = 0$), easier to adsorb ($0 < R_L < 1$), linear ($R_L = 1$) or difficult to adsorb ($R_L > 1$) [34,35]. The R_L within the initial concentration range of HRP can be calculated by the fitting equation to be 0.291–0.860, so PVDAT nanoparticles belong to the type that is easier to adsorb HRP. Under the premise of electrostatic repulsion, HRP can be easily adsorbed, which also proves the dominant role of hydrogen bond between PVDAT nanoparticles and HRP in the water phase.

Keep the pH at 6 and the ionic strength at 0.1 mol/L unchanged. Because the HRP adsorption was relatively stable under low concentration conditions, 100 μg/mL HRP solutions were selected to test the adsorption ratio of nanoparticles to HRP during the adsorption time of 5–90 min. Fig. 13 showed that as the adsorption time increased, the adsorption percentage gradually increased and eventually tended to equilibrium. This is because in the early stage of adsorption, the

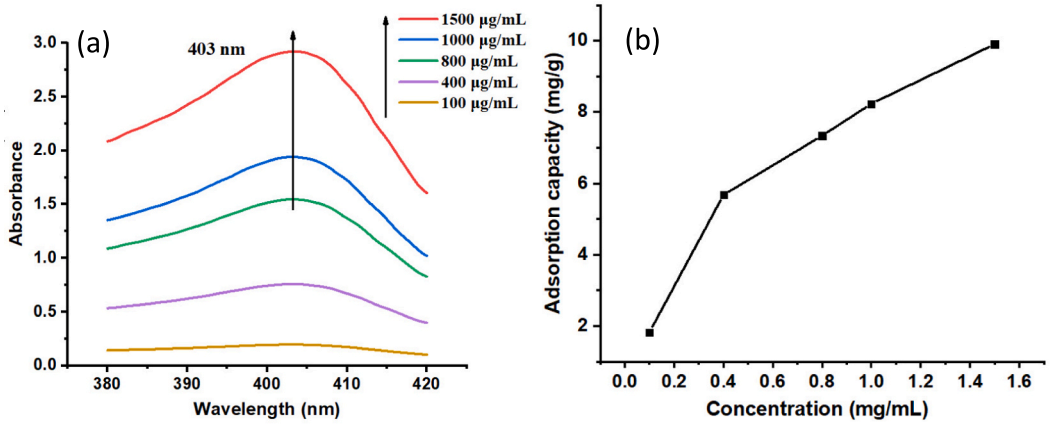

Fig. 11. The adsorption capacity of HRP on PVDAT nanoparticles: (a) UV spectrum, (b) The relationship curve between adsorption capacity and HRP concentration.

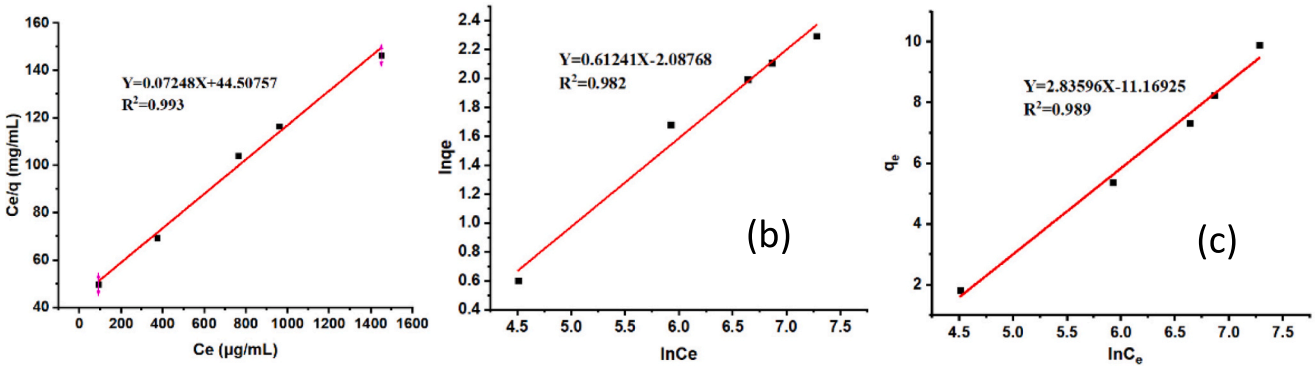

Fig. 12. HRP adsorption isotherm equations fitting: (a) Langmuir, (b) Freundlich, (c) Temkin.

hydrogen bonding sites on the surface of the nanoparticles are basically in a vacant state. At this stage, due to the synergy of hydrophobic interaction and hydrogen bonding, HRP will quickly be adsorbed to the surface of the nanoparticles. With the gradual increase in the amount of adsorption, the increase in the surface coverage of the nanoparticles leads to a decrease in hydrogen bonding sites, and the adsorption rate begins to decrease. Eventually, the entire system stabilizes and reaches an adsorption equilibrium. From the experimental results, the entire adsorption process takes about 35 min to reach the maximum adsorption percentage. So, the adsorption process takes about 35 min to reach the maximum adsorption percentage. Compared with other adsorbent materials, the whole adsorption process is relatively short, for example, the chitosan cotton composite prepared by Salman et al. has an equilibrium time of up to 90 min on substrates [36].

The size of the nanoparticles also plays an important role in the adsorption process of proteins [37]. The adsorption concentration of HRP using PVDAT nanoparticles with a particle size of 120 nm, 150 nm and 240 nm under different initial concentrations of HRP was shown in Fig. 14. Under the same particle size, the adsorption concentration of HRP increased with the increase of the initial concentration of HRP. At the same concentration, the adsorption concentration increased with the decrease of the particle size, and the higher the concentration, the more obvious the difference. Because the smaller the particle size of PVDAT nanoparticles, the larger the specific surface area and the stronger the adsorption capacity. This also fully proves the advantages of nanomaterials in adsorption.

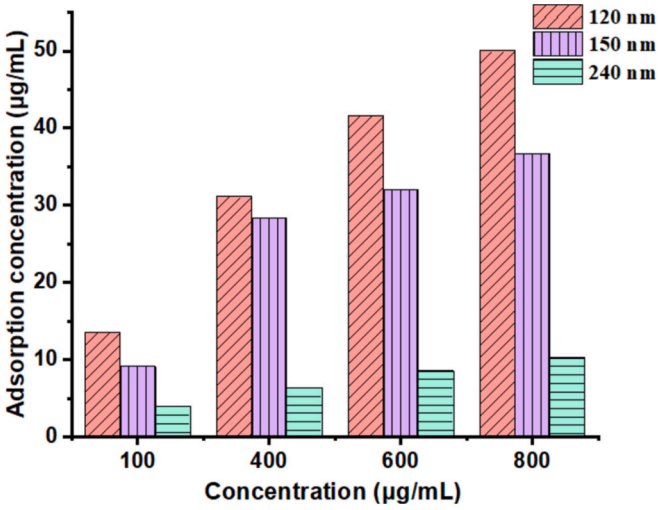

Fig. 14. The adsorption of PVDAT nanoparticles with different diameters to different concentrations of HRP.

3.3. Activity of adsorbed HRP

When it is not possible to study the activity of enzymes directly and sensitively, it can be demonstrated by indirect methods, such as the concentration of complexes or catalytic substrates using UV–Vis photometry [38,39]. Under HRP catalysis, the hydrogen donor substrate TMB will be oxidized by H_2O_2 to produce a blue product, which has two absorption peaks at 370 nm and 650 nm, as shown in Fig. 15(a) Moreover, with the extension of the reaction time, the UV absorption intensity of the product will gradually increase. Fig. 15(b) showed the curve of the absorbance of the reaction product obtained at a

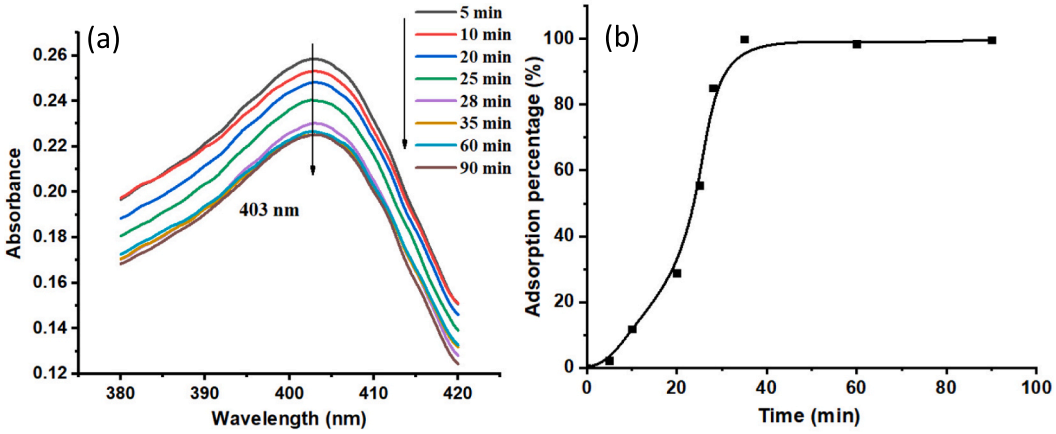

Fig. 13. The adsorption kinetics of HRP on PVDAT nanoparticles: (a) UV spectrum, (b) The relationship between adsorption capacity and time.

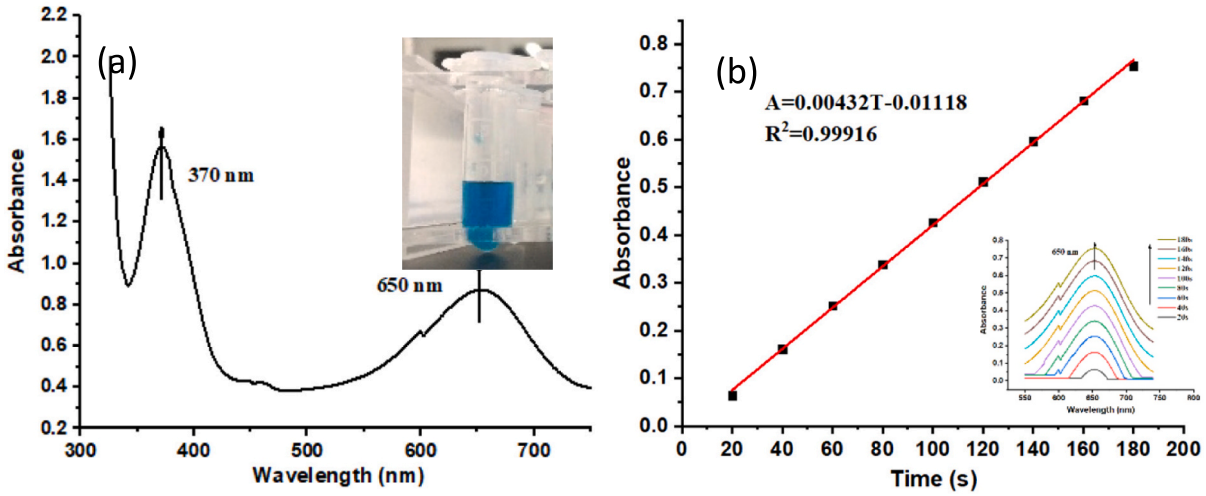

Fig. 15. HRP reaction product results: (a) UV absorption and (b) fitting curve.

wavelength of 650 nm with the reaction time. The fitting results showed that the correlation coefficient R^2 was 0.99916, so the absorbance of the product in the early stage of the reaction had a good linearity with the reaction time. This was because the concentration of the enzyme was extremely low relative to the concentration of the substrate when the reactants were prepared, which can keep the substrate concentration approximately constant in the initial reaction system. Therefore, it is proved that in the early stage of the reaction, the reduction of the substrate in the system had a negligible effect on the enzyme reaction rate.

Fig. 16(a) showed the catalytic reaction process curve of different concentrations of HRP, which specifically reflected the curve of absorbance at 650 nm with reaction time, from which the activity value of HRP can be calculated. It could be seen from the above that at the beginning of the reaction, the substrate concentration can be approximated as a fixed value, and the reaction product had a linear relationship with time. Therefore, the slope of the reaction process curve can be used to express the enzyme activity [40]. Fig. 16(b)showed the relationship between HRP concentration and activity. It can be seen from the figure that there was still a good linear relationship between HRP concentration and activity: $S = 0.14348C + 0.11555$, $R^2 = 0.99915$. Where S represents HRP activity and C is HRP concentration. Therefore, this equation can be used to quantify the content of active enzyme by measuring the slope of the reaction process curve corresponding to the product to be tested.

Under different initial concentrations of HRP, the UV process of the enzyme-catalyzed reaction of HRP adsorbed on PVDAT nanoparticles was tested, as shown in the Fig. 17(a). From the UV diagram, the slopes of the enzyme protein from low to high concentrations were 1.0974, 2.4301, 2.9580, 3.0687, 2.9278, respectively. The slopes were taken into the above obtained enzyme reaction process fitting equation to obtain the concentration of active enzyme at each concentration. Then, comparing the concentration of enzyme with the concentration of adsorbed enzyme can get the proportion of active enzyme under different initial concentration of HRP. As shown in Fig. 17(b), the proportion of active enzymes gradually decreased from 74.99 %, 61.32 %, 54.85 %, 51.33 % to 39.58 % as the concentration increased [41]. In addition, under the premise that the surface structure of the enzyme protein itself was relatively complex, after multiple interactions, the system may become unstable and lead to a part of the enzyme conformation change. This also explained why the adsorption capacity increased sharply when the concentration was high to a certain level during adsorption, because some of the adsorbed enzymes had lost their activity, leading to multilayer adsorption. The results showed that PVDAT nanoparticles had an obvious adsorption effect on the lower concentration of HRP. Although the adsorption capacity was small at low concentrations, it is more important that the enzyme protein was stably adsorbed through hydrophobic and hydrogen bonding during the adsorption process, and the natural conformation and biological activity of the enzyme were basically not affected. This has laid a certain foundation for the application of PVDAT nanoparticles in the field of biosensors and as a solid-phase carrier for protein MIP.

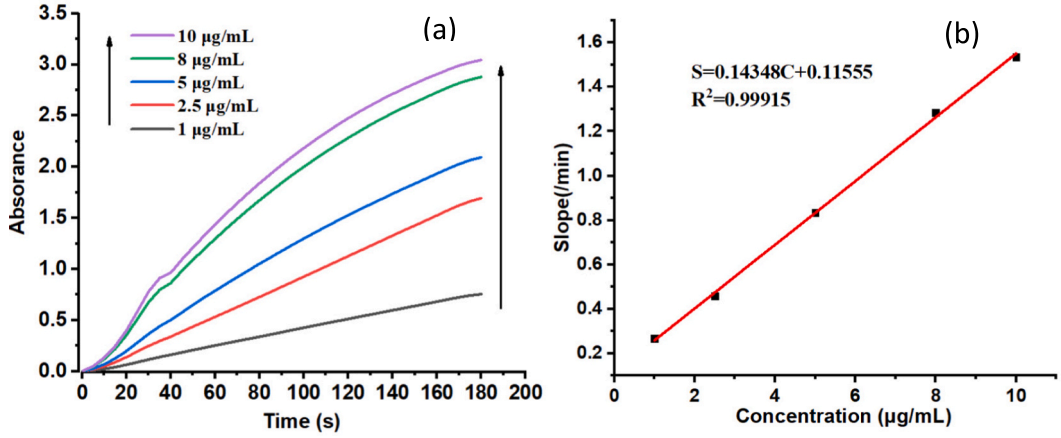

Fig. 16. HRP reaction process curve: (a) UV absorption and (b) fitting curve.

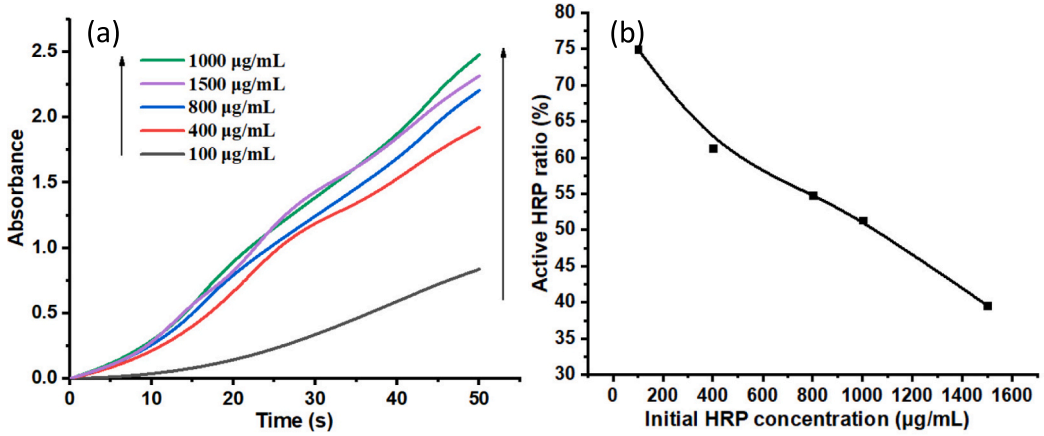

Fig. 17. Enzyme reaction process diagram adsorbed on PVDAT nanoparticles under different HRP concentrations: (a) UV absorption and (b) active enzyme ratio diagram.

4. Conclusions

Hydrogen bonding dominated adsorption of proteins with high directionality and stability in aqueous media. However, a challenge exists in aqueous media because water molecules are an effective competitor which could weaken or even destroy the H-bonding between the proteins and functional polymers. Hydrophobic property of 2-vinyl-4,6-diamino-1,3,5-triazine (VDAT) polymer nanoparticles (PVDAT) could built stable hydrophobic hydrogen bonding with protein to produce adsorption in aqueous environments. An innovative semi-continuous precipitation polymerization was used to synthesize PVDAT nanoparticles with different size (120 nm, 150 nm and 240 nm). VDAT oligomers formed at the early polymerization stage, and then precipitated from the aqueous phase to form nuclei which then grew by adsorbing more and more VDAT oligomers/polymers. A maximum adsorption capacity achieved 13.80 mg/g of HRP which accorded with a Langmuir monolayer adsorption. Specially, the ELISA analysis indicated that up to 74.99 % of the HRP adsorbed by PVDAT were biocatalytic active. The hydrophobic hydrogen bonding dominated adsorption of protein might be used in enzyme biosensor, medical diagnostic assay and sewage treatment.

CRediT authorship contribution statement

Xiaotao Wang: Writing – original draft, Supervision, Funding acquisition. **Chuan Xu:** Formal analysis, Data curation, Conceptualization. **Feiyang Xiao:** Validation, Data curation. **Xiangning Yan:** Visualization, Project administration. **Chak-Yin Tang:** Writing – review & editing, Resources. **Huiling Guo:** Supervision, Investigation. **Wing-Cheung Law:** Writing – review & editing, Supervision, Funding acquisition, Formal analysis.

Declaration of competing interest

The authors declare that they have no known competing financial interests or personal relationships that could have appeared to influence the work reported in this paper.

Acknowledgement

This work was supported by the Natural National Science Foundation of China [51303049 and 31871442] and grant from the Research Committee of The Hong Kong Polytechnic University under project account code G-UARP.

Appendix A. Supplementary data

Supplementary data to this article can be found online at https://doi.org/10.1016/j.reactfunctpolym.2025.106156.

Data availability

The raw/processed data required to reproduce these findings cannot be shared at this time due to legal or ethical reasons.

References

[1] M.S. Hossain, M.A. Shenashen, E. Awual, A.I. Rehan, A.I. Rasee, R.M. Waliullah, K. T. Kubra, M.S. Salman, M.C. Sheikh, M.N. Hasan, M.M. Hasan, A. Islam, M. A. Khaleque, H.M. Marwani, K.A. Alzahrani, A.M. Asiri, M.M. Rahman, M. R. Awual, Benign separation, adsorption, and recovery of rare-earth Yb(III) ions with specific ligand-based composite adsorbent, Process. Saf. Environ. Prot. 185 (2024) 367–374.
[2] H.H. Nguyen, M. Kim, An overview of techniques in enzyme immobilization, Appl. Sci. Converg. Technol. 26 (6) (2017) 157–163.
[3] H. Zhang, J. Luo, S. Li, Y. Wei, Y. Wan, Biocatalytic membrane based on Polydopamine coating: a platform for studying immobilization mechanisms, Langmuir 34 (8) (2018) 2585–2594.
[4] K. Matsuura, T. Saito, T. Okazaki, S. Ohshima, M. Yumura, S. Iijima, Selectivity of water-soluble proteins in single-walled carbon nanotube dispersions, Chem. Phys. Lett. 429 (4) (2006) 497–502.
[5] I. Ahmed, Z. Hasan, G. Lee, H.J. Lee, S.H. Jhung, Contribution of hydrogen bonding to liquid-phase adsorptive removal of hazardous organics with metal-organic framework-based materials, Chem. Eng. J. 430 (2022) 132596.
[6] S. Guo, Z. Zou, Y. Chen, X. Long, M. Liu, X. Li, J. Tan, R. Chen, Synergistic effect of hydrogen bonding and π-π interaction for enhanced adsorption of rhodamine B from water using corn straw biochar? Environ. Pollut. 320 (2023) 121060.
[7] Y. Zhang, B. Gao, Z. Xu, Adsorption properties of polyvinyl-alcohol-grafted particles toward Genistein driven by hydrogen-bond interaction, J. Phys. Chem. B 117 (18) (2013) 5730–5736.
[8] K.-D. Zhang, D. Ajami, J. Rebek, Hydrogen-bonded capsules in water, J. Am. Chem. Soc. 135 (48) (2013) 18064–18066.
[9] D. Liu, J.-X. Bardaud, Z. Imani, S. Robin, E. Gloaguen, V. Brenner, D.J. Aitken, M. Mons, Length-dependent transition from extended to folded shapes in short oligomers of an Azetidine-based α-amino acid: the critical role of NH•••N H-bonds, Molecules 28 (13) (2023) 5048.
[10] W. Kabsch, C. Sander, Dictionary of protein secondary structure: pattern recognition of hydrogen-bonded and geometrical features, Biopolymers 22 (12) (1983) 2577–2637.
[11] N. Wang, Y. Han, Y. Liu, T. Bai, H. Gao, P. Zhang, W. Wang, W. Liu, High-strength hydrogel as a reusable adsorbent of copper ions, J. Hazard. Mater. 213 (2012) 258–264.
[12] N. Wang, L. Tang, W. Liu, High-strength smart hydrogels as a versatile platform for surface-mediated gene delivery, Nanomedicine 12 (2) (2016), 462-462.
[13] X. Xie, L. Huang, Z. Liu, W. Xie, X. Wang, Synthesis of poly(2-vinyl-4,6-diamino-1,3,5-triazine) nanoparticles by semi-continuous precipitation polymerization, characterization and application to bovine hemoglobin adsorption, React. Funct. Polym. 141 (2019) 58–67.
[14] M.R. Awual, New type mesoporous conjugate material for selective optical copper (II) ions monitoring & removal from polluted waters, Chem. Eng. J. 307 (2017) 85–94.

[15] E. Awual, M.S. Salman, M.M. Hasan, M.N. Hasan, K.T. Kubra, M.C. Sheikh, A. I. Rasee, A.I. Rehan, R.M. Waliullah, M.S. Hossain, H.M. Marwani, A.M. Asiri, M. M. Rahman, A. Islam, M.A. Khaleque, M.R. Awual, Ligand imprinted composite adsorbent for effective Ni(II) ion monitoring and removal from contaminated water, J. Ind. Eng. Chem. 131 (2024) 585–592.
[16] Y. Jiang, W. Tang, J. Gao, L. Zhou, Y. He, Immobilization of horseradish peroxidase in phospholipid-templated titania and its applications in phenolic compounds and dye removal, Enzym. Microb. Technol. 55 (2014) 1–6.
[17] C. Sheikh, M. Hasan, N. Hasan, S. Salman, K.T. Kubra, M.E. Awual, R.M. Waliullah, A.I. Rasee, A.I. Rehan, M.S. Hossain, H.M. Marwani, A. Islam, A. Khaleque, R. Awual, Toxic cadmium(II) monitoring and removal from aqueous solution using ligand-based facial composite adsorbent, J. Mol. Liq. 389 (2023) 122854.
[18] S. Liu, S. Qiao, T. Yan, X. Li, S. Yu, H. Sun, J. Xu, J. Liu, Giant nanotubes equipped with horseradish peroxidase active sites: a powerful nanozyme co-assembled from supramolecular amphiphiles for glucose detection, Chem. Eng. J. 429 (2022) 132592.
[19] G.A. Valencia, L.C. de Oliveira Vercik, A. Vercik, A new conductometric biosensor based on horseradish peroxidase immobilized on chitosan and chitosan/gold nanoparticle films, J. Polym. Eng. 34 (7) (2014) 633–638.
[20] N. Sawa, T. Masuda, T. Mizui, Isocyanuric acid adduct of 2-vinyl-4,6-diamino-S-triazine, process for synthesis of said adduct and process for hardening polyepoxy resin with said adduct, 2024. EP0151530B1.
[21] V.V. Figueiredo, E.L.F. Vianna, B.S. Lima, F. Garcia-Villen, L.C. Bertolino, L. S. Spinelli, C. Viseras, Brazilian palygorskite as an alternative to commercial adsorbents for methylene blue: a discussion about composition, morphology and pore profile, Microporous Mesoporous Mater. 366 (2024) 112957.
[22] D. Liang, B.-Y. Ji, Y. Wang, X. Li, W.-Y. Gao, Effect of activated carbon microstructure and adsorption mechanism on the efficient removal of chlorophyll a and chlorophyll b from *Andrographis paniculata* extract, Sci. Rep. 13 (1) (2023) 21930.
[23] L.N. Ndlovu, K.E. Mokubung, C. Donga, N.N. Gumbi, A.K. Mishra, E.N. Nxumalo, S. B. Mishra, Dual-functional Polyvinylidene fluoride Beta Cyclodextrin-grafted graphene oxide mixed matrix membranes for removal of anionic azo dyes, J. Inorg. Organomet. Polym. Mater. 34 (5) (2024) 2219–2241.
[24] I. Langmuir, The constitution and fundamental properties of solids and liquids. Part II.—liquids, J. Frankl. Inst. 184 (5) (1916) 102–105.
[25] A.I. Rasee, E. Awual, A.I. Rehan, M.S. Hossain, R.M. Waliullah, K.T. Kubra, M. C. Sheikh, M.S. Salman, M.N. Hasan, M.M. Hasan, H.M. Marwani, A. Islam, M. A. Khaleque, M.R. Awual, Efficient separation, adsorption, and recovery of samarium(III) ions using novel ligand-based composite adsorbent, Surf. Interfaces 41 (2023) 103276.
[26] X. Xie, L. Huang, Z.F. Liu, W.H. Xie, X.T. Wang, Synthesis of poly(2-vinyl-4,6-diamino-1,3,5-triazine) nanoparticles by semi-continuous precipitation polymerization, characterization and application to bovine hemoglobin adsorption, React. Funct. Polym. 141 (2019) 58–67.
[27] J.S. Downey, R.S. Frank, W.-H. Li, H.D.H. Stöver, Growth mechanism of poly (divinylbenzene) microspheres in precipitation polymerization, Macromolecules 32 (9) (1999) 2838–2844.
[28] M.N. Hasan, M.S. Salman, M.M. Hasan, K.T. Kubra, M.C. Sheikh, A.I. Rehan, A. I. Rasee, M.E. Awual, R.M. Waliullah, M.S. Hossain, A. Islam, S. Khandaker, A.K. D. Alsukaibi, H.M. Alshammari, M.R. Awual, Assessing sustainable lutetium(III) ions adsorption and recovery using novel composite hybrid nanomaterials, J. Mol. Struct. 1276 (2023) 134795.
[29] J. Kreusser, H. Hasse, F. Jirasek, Adsorption of bovine serum albumin on a mixed-mode resin-influence of salts and the pH value, Adsorpt. J. Int. Adsorpt. Soc. 29 (3–4) (2023) 163–176.
[30] M.R. Awual, M.N. Hasan, M.M. Hasan, M.S. Salman, M.C. Sheikh, K.T. Kubra, M. S. Islam, H.M. Marwani, A. Islam, M.A. Khaleque, R.M. Waliullah, M.S. Hossain, A. I. Rasee, A.I. Rehan, M.E. Awual, Green and robust adsorption and recovery of europium(III) with a mechanism using hybrid donor conjugate materials, Sep. Purif. Technol. 319 (2023) 124088.
[31] M.M. Hasan, M.S. Salman, A.I. Rehan, M.E. Awual, A.I. Rasee, R.M. Waliullah, M. S. Hossain, K.T. Kubra, M.C. Sheikh, M.A. Khaleque, H.M. Marwani, A. Islam, M. R. Awual, Facial conjugate adsorbent for sustainable Pb(II) ion monitoring and removal from contaminated water, Colloids Surf. A Physicochem. Eng. Asp. 673 (2023) 131794.
[32] M.M. Hasan, K.T. Kubra, M.N. Hasan, M.E. Awual, M.S. Salman, M.C. Sheikh, A. I. Rehan, A.I. Rasee, R.M. Waliullah, M.S. Islam, S. Khandaker, A. Islam, M. S. Hossain, A.K.D. Alsukaibi, H.M. Alshammari, M.R. Awual, Sustainable ligand-modified based composite material for the selective and effective cadmium(II) capturing from wastewater, J. Mol. Liq. 371 (2023) 121125.
[33] J.-B. Liu, Y. Wang, T.-T. Su, B. Li, S.-S. Tang, R.-F. Jin, Theoretical and experimental studies on the performances of barbital-imprinted systems, J. Sep. Sci. 38 (23) (2015) 4105–4110.
[34] M.M. Ayad, A.A. El-Nasr, Adsorption of cationic dye (methylene blue) from water using polyaniline Nanotubes Base, J. Phys. Chem. C 114 (34) (2010) 2177–2187.
[35] M.A. Wahab, S. Jellali, N. Jedidi, Ammonium biosorption onto sawdust: FTIR analysis, kinetics and adsorption isotherms modeling, Bioresour. Technol. 101 (14) (2010) 5070–5075.
[36] M.S. Salman, M.C. Sheikh, M.M. Hasan, M.N. Hasan, K.T. Kubra, A.I. Rehan, M. E. Awual, A.I. Rasee, R.M. Waliullah, M.S. Hossain, M.A. Khaleque, A.K. D. Alsukaibi, H.M. Alshammari, M.R. Awual, Chitosan-coated cotton fiber composite for efficient toxic dye encapsulation from aqueous media, Appl. Surf. Sci. 622 (2023) 157008.
[37] K. Das, S. Kundu, Adsorption and conformation variation of BSA protein with the size variation of the metallic nanoparticles in LB film, Colloids Surf. A Physicochem. Eng. Asp. 468 (2015) 56–61.
[38] M.S. Salman, M.N. Hasan, M.M. Hasan, K.T. Kubra, M.C. Sheikh, A.I. Rehan, R. M. Waliullah, A.I. Rasee, M.E. Awual, M.S. Hossain, A.K.D. Alsukaibi, H. M. Alshammari, M.R. Awual, Improving copper(II) ion detection and adsorption from wastewater by the ligand-functionalized composite adsorbent, J. Mol. Struct. 1282 (2023) 135259.
[39] Y. Yu, Y. Wang, M. Li, Reliable method for the detection of horseradish peroxidase activity and enzyme kinetics, Analyst 144 (4) (2019) 1442–1447.
[40] Q. Wang, M. Zhuang, B. Yu, L. Zhang, X. Chen, TMB method study of peroxidase activity in pork, Anal. Lab. 07 (2007) 14–18.
[41] P. Koegler, A. Clayton, H. Thissen, G.N.C. Santos, P. Kingshott, The influence of nanostructured materials on biointerfacial interactions, Adv. Drug Deliv. Rev. 64 (15) (2012) 1820–1839.